Biomaterials Science

ROYAL SOCIETY OF CHEMISTRY

PAPER

View Article Online
View Journal | View Issue

Cite this: *Biomater. Sci.*, 2023, **11**, 2383

In situ forming double-crosslinked hydrogels with highly dispersed short fibers for the treatment of irregular wounds†

Maidi Wang,‡[a] Jingtao Du,‡[a] Mengya Li,[a] Filippo Pierini,[b] Xiaoran Li,*[a] Jianyong Yu[a] and Bin Ding*[a]

In situ forming injectable hydrogels hold great potential for the treatment of irregular wounds. However, their practical applications were hindered by long gelation time, poor mechanical performance, and a lack of a natural extracellular matrix structure. Herein, amino-modified electrospun poly(lactic-*co*-glycolic acid) (APLGA) short fibers with uniform distribution were introduced into gelatin methacrylate/oxidized dextran (GM/ODex) hydrogels. In comparison with the fiber aggregation structure in the PLGA fiber-incorporated hydrogels, the hydrogels with APLGA fibers possessed a uniform porous structure. The highly dispersed APLGA short fibers accelerated the sol–gel phase transition of the hydrogel due to the formation of dynamic Schiff-base bonds between the fibers and hydrogels. Furthermore, in combination with UV-assisted crosslinking, a rapid gelation time of 90 s was achieved for the double-crosslinked hydrogels. The addition of APLGA short fibers as fillers and the formation of the double-crosslinking network enhanced the mechanical performance of the hydrogels. Furthermore, the fiber–hydrogel composites exhibited favorable injectability, excellent biocompatibility, and improved cell infiltration. *In vivo* assessment indicated that the GM/ODex-APLGA hydrogels successfully filled the full-thickness defects and improved wound healing. This work demonstrates a promising solution for the treatment of irregular wounds.

Received 17th November 2022,
Accepted 25th January 2023

DOI: 10.1039/d2bm01891h

rsc.li/biomaterials-science

1. Introduction

Skin trauma with irregular shapes inevitably occurs in our daily life all the time. Acute and chronic wounds significantly affect human health and even lead to death. Therefore, the development of an effective wound dressing has received extensive attention in the biomedical field.[1–3] It has been well established that a favorable microenvironment plays a significant role in wound healing and tissue remodeling.[4,5] At present, various wound dressings have been developed to expedite the repair of skin wounds, including functional gauze,[6] membranes,[7] sponges,[8] hydrocolloids,[9] polymersomes,[10] and hydrogels.[11] Among them, hydrogel dressings have become increasingly popular due to oxygen permeability, wound exudate absorption property, and moisture retention characteristics.[12,13] However, the conventional hydrogel dressings are in the form of sheets, and they should be prepared in advance, resulting in imperfect coverage of irregular wounds and incomplete filling of deep wounds.

Therefore, *in situ* formed dressings bring breakthroughs for treating irregular wounds. However, *in situ* formed hydrogel dressings suffer from long gelation time, poor mechanical properties, and a lack of a natural extracellular matrix (ECM)-like structure. Various injectable *in situ* forming hydrogels have been developed based on the Schiff-base reaction,[13] Diels–Alder reaction,[14] photo-crosslinking reaction,[15] and so on. To address the limitation in mechanical properties, micro/nanomaterials have been incorporated into polymer networks. The mechanical properties of composite hydrogels could be readily manipulated by regulating the concentration and size of the incorporated materials and molecular weight of the polymer matrix.[16,17] Various materials, including carbon-based nanomaterials (carbon nanotubes, graphene oxide and nanodiamonds),[18–21] metal-based micro/nanomaterials (gold),[22,23] inorganic nanomaterials (nanosilicates and hydroxyapatite),[24,25] and polymeric nanomaterials (chitosan nanoparticles and cellulose nanofibrils)[26,27] have been

[a]*Innovation Center for Textile Science and Technology, College of Textiles, Donghua University, Shanghai 201620, China. E-mail: xiaoranli@dhu.edu.cn, binding@dhu.edu.cn*
[b]*Department of Biosystems and Soft Matter, Institute of Fundamental Technological Research, Polish Academy of Sciences, Warsaw 02-106, Poland*

†Electronic supplementary information (ESI) available. See DOI: https://doi.org/10.1039/d2bm01891h

‡These authors contributed equally to this work.

employed to fabricate composite hydrogels with specific performance and functions. Furthermore, micro/nanomaterial-reinforced hydrogels possess synergistic and unique capabilities, which are superior to those of pristine hydrogels.[28] However, non-biodegradability and toxicity have become concerns. In addition, the nanoparticle-incorporated hydrogels are not able to mimic the natural ECM, resulting in unfavorable cell adhesion and growth. The cellulose nanofibril-embedded hydrogels resemble the 3D fibrous structure of the ECM. However, the preparation of cellulose nanofibrils requires a complex procedure and the chemically inert surface cannot be easily functionalized, which hinder their applications.[29,30]

Electrospinning provides a facile and enabling platform to fabricate fibers with diameters ranging from a few nanometers to several micrometers, which can imitate the size and structure of the natural ECM.[31] In addition, distinct features in terms of diversity in composition, control of fiber size, ease of surface functionalization, *etc*. have made electrospun nanofibrous materials become promising candidates in biomedical applications.[32–34] Fibrous membrane-enhanced hydrogels have been reported by layer-by-layer assembly.[35] For example, Stocco *et al.*[36] developed a reinforced hydrogel by introducing multilayers of aligned electrospun polycaprolactone (PCL)/carbon nanotube nanofibrous membranes into a collagen-based hydrogel, which dramatically strengthened the mechanical performance of the composite hydrogels. Nevertheless, because of the weak interaction between the fiber and matrix, these composite hydrogels may delaminate resulting in an unstable structure. More importantly, these scaffolds cannot be injected into the wound sites. Significant advances have been made in the development of short fiber-incorporated hydrogels *via* the inclusion of segmented fibers into hydrogels. The short fiber-embedded hydrogels are able to meet the requirement of ECM recapitulation and injectable capability simultaneously. Recently, further progress has been made to improve the structural integrity *via* the introduction of interfacial bonding between fiber segments and hydrogels. Li *et al.*[37] prepared a covalently conjugated short fiber–hydrogel composite. It was found that the incorporation of short fibers could not only improve the mechanical properties but also promote a sequence of biological properties, including cell infiltration, macrophage regulation and blood vessel formation. Despite the progress, the short fiber-embedded hydrogels pose several limitations. The addition of fibers would hinder the sol–gel phase transition process of the *in situ* forming hydrogels. In addition, fiber aggregation normally occurs, which significantly affects the mechanical properties of the composite hydrogels. Therefore, developing short fiber-reinforced *in situ* forming hydrogels with favorable gelling time and mechanical properties is highly desirable.

Herein, we developed a gelatin methacrylate/oxidized dextran (GM/ODex) hydrogel incorporated with highly dispersed amino-modified poly(lactic-*co*-glycolic acid) (APLGA) electrospun fiber segments (Scheme 1). In this design, the APLGA fiber segments were utilized as fillers and reacted with ODex chains to form Schiff-base-bonds. The dynamic Schiff-base bonds at the hydrogel–fiber interface were beneficial for even dispersion of short fibers in the hydrogel and sol–gel transition. The homogeneously distributed short fiber, in combination with a double-crosslinking network composed of dynamic bonds between short fibers and the hydrogel and photo-crosslinked GM in the main hydrogel, contributed to the improved mechanical properties. Besides, these hydrogel composites showed good biocompatibility and improved cell infiltration. The *in vivo* experiments demonstrated that the hydrogel composites facilitated wound healing. Overall, we developed an *in situ* forming double-crosslinked hydrogel with highly dispersed short fibers, which has opened up more possibilities in the field of wound dressing.

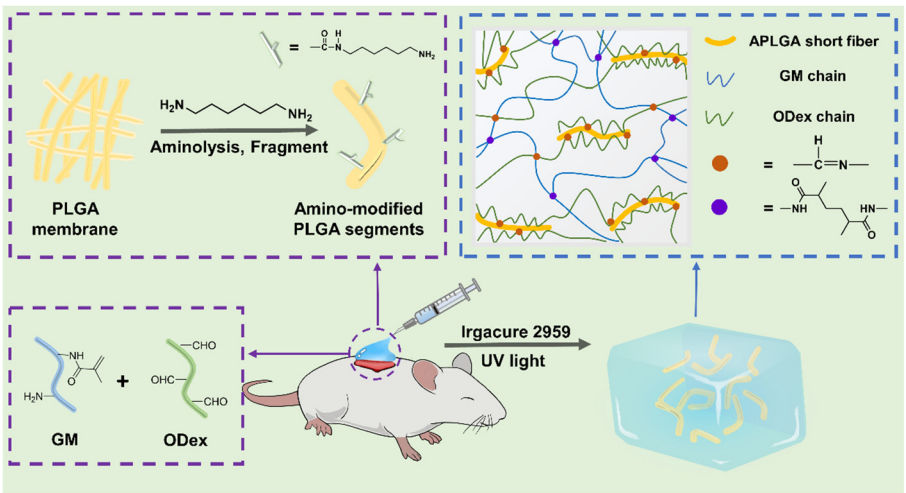

Scheme 1 Schematic illustration of preparation of double-crosslinked hydrogels with highly dispersed APLGA short fibers and application of the *in situ* forming short fiber–hydrogel composite for wound healing in rats.

2. Experimental section

2.1. Materials

Hexafluoroisopropanol (HFIP, 99.5%) and gelatin (type A, porcine) were purchased from Shanghai Macklin Biochemical Co., Ltd (China). PLGA (LA/GA = 75/25) was obtained from Daigang Biological Engineering Co., Ltd (Jinan, China). Methacrylic anhydride (MA), dextran (M_w = 70 000), 1,6-hexamethylenediamine (AR, 99.0%), and poly(vinyl alcohol) (PVA) (87.0–89.0 mol%) were obtained from Shanghai Aladdin Biochemical Technology Co., Ltd (China). Sodium periodate ($NaIO_4$, AR, 99.5%) was provided by Rhawn (Shanghai, China). Ethylene glycol (99%) was purchased from Infinity Scientific (Shanghai, China). Deionized water was used throughout.

2.2. Preparation and characterization of short APLGA fibers

The PLGA fibers were prepared by the electrospinning technique. Briefly, PLGA was dissolved in HFIP and kept stirring for 48 h to get the PLGA solution (20% w/v). Then, the PLGA solution was electrospun, and the feeding rate, voltage and needle-to-collector distance were set at 1.0 mL h^{-1}, 9 kV, and 15 cm respectively.

The APLGA short fibers were prepared by aminolysis treatment followed by homogenizing. In brief, the electrospun PLGA fibrous mats were immersed in 2% w/v 1,6-hexanediamine solution and treated at 37 °C for 1 h, followed by washing with plenty of DI water 3 times. Subsequently, the APLGA mats were cut into pieces and added into 0.5% w/v solution of PVA, followed by homogenization at 8000 rpm. The suspensions were ultimately washed with DI water to remove PVA followed by lyophilization. Similarly, the PLGA fibers without aminolysis treatment were cut, homogenized, and lyophilized to get PLGA short fibers.

2.3. Synthesis of GM and ODex

GM was synthesized according to previous study.[38] In brief, gelatin (6 g) was added in PBS (50 mL) at 55 °C, followed by stirring until complete dissolution. Then, MA (5 mL) was dropped to the above gelatin solution slowly at a rate of 1 mL min^{-1} and the solution was kept stirring at 50 °C for 3 h. Then, PBS (300 mL) was added to terminate the reaction. The mixture was dialyzed using a dialysis bag (MWCO = 8–14 kDa) for 5 d and lyophilized for 2 d. The degree of substitution of GM was calculated according to the previous report.[39]

ODex was synthesized following the previous report.[40] Briefly, dextran (5 g) was dissolved in DI water (125 mL) at a concentration of 4% w/v. Subsequently, $NaIO_4$ (5 g) was added followed by stirring for 3.5 h in a dark environment. Then, the unreacted $NaIO_4$ was quenched by adding ethylene glycol (3 mL). The solution was dialyzed (MWCO = 8–14 kDa) using DI water for 3 d, followed by lyophilization. Then, the hydroxylamine hydrochloride titration method was used to detect the oxidation degree of ODex.[41]

2.4. Preparation of fiber–hydrogel composites

The fiber–hydrogel composites were fabricated by mixing short fibers with hydrogel precursors. GM solution was prepared by dissolving GM in DI water at 50 °C. Then, Odex, photoinitiator Irgacure 2959 and short fibers were added successively to obtain a solution containing 10% w/v GM, 2% w/v Odex, 0.5% w/v Irgacure 2959 and 1% w/v short fibers. Next, the fiber–hydrogel precursor was prepared by ultrasonic treatment for 10 min. Finally, the hydrogels were gelled completely by UV irradiation.

2.5. Characterization of short fibers and hydrogels

The morphology of electrospun short fibers and the microstructure of the hydrogels were observed by scanning electron microscopy (SEM, Vega 3, Tescan, Czech). The functional groups and constituent elements of the electrospun fibers were characterized by Fourier transform infrared spectroscopy (FT-IR, Nicolet iN10 MX, Thermo Scientific, America) and X-ray photoelectron spectroscopy (XPS, EscaLab 250Xi, Thermo Scientific, America). A contact angle goniometer (SL200KS, KINO, America) was used to determine the water contact angle (WCA) of the electrospun membrane. In brief, 5 μL droplets of DI water were deposited on the mats, and the droplet images were recorded with a high-resolution camera. The ImageJ software was used to calculate the WCA. The chemical structure of GM and ODex was determined by ^{1}H-NMR (Avance III HD600 MHz, Bruker, Switzerland).

2.6. Gelation test

A vial inversion test was used to determine the gelation time of the hydrogels. The GM/ODex solution and short fibers were gently mixed, and maintained at room temperature. The sol–gel transition process was observed by vial tilting every 5 min. The gelation time was obtained when the gel remained non-flowing in the inverted vial. For GM/ODex-APLGA, the gelation time under UV irradiation was also recorded.

2.7. Swelling test

To assess swelling behavior, the lyophilized hydrogel samples were immersed in PBS. After equilibration at 37 °C for a certain time, the hydrogels were taken out, and excessive PBS was removed by filter paper, followed by weighing. The swelling ratio was calculated using the following formula:

$$\text{Swelling ratio}(\%) = \frac{W_t - W_0}{W_0} \times 100\%$$

where W_0 and W_t are the initial weight and the weight at a specific time point, respectively.

2.8. Rheological measurements

The rheological property of fiber–hydrogel composites was evaluated using a rheometer (MARS 60, Haake, German). The prepared samples were placed on the center of parallel plates. The strain sweep test was conducted at a frequency of 1 Hz with strains ranging from 0.1% to 100%. Moreover, 1% constant strain and frequency in the range of 0.01–10 Hz were employed to conduct the frequency sweep test.

2.9. Compression test

The compression test of fiber–hydrogel composites was performed using a universal testing machine (HY-940FS, Hengyu, China) with a load cell of 200 N at a constant rate (1 mm min^{-1}). The compressive stress–strain curves were obtained, and the compressive strength was defined as the stress at the fracture during the test. The compressive modulus was calculated by linear fitting from 10 to 15% strain of the stress–strain curves.

2.10. *In vitro* cytocompatibility

Mouse fibroblast cells (L929) were used to assess the cytocompatibility of the fiber–hydrogel composites. Cell viability was detected *via* live/dead staining. All samples were sterilized by immersion in 75% ethanol and UV irradiation. Subsequently, 3×10^4 fibroblasts were cultured on the surface of each hydrogel. After incubation in 5% CO_2 at 37 °C for 3 d, samples were stained with live/dead assay (calcein-AM/ethidium homodimer-1) for 30 min. The fluorescence images were obtained *via* a confocal laser scanning microscope (LSM 900, Zeiss, Germany). Cell proliferation during 7 days was evaluated by a CCK-8 assay. At indicated time points, the medium was displaced by DMEM medium (200 μL) containing CCK-8 (20 μL), followed by incubation for 3 h. The OD values of the supernatant were determined at 450 nm wavelength *via* a microplate reader.

2.11. *In vivo* wound healing performance

To evaluate the efficacy of composite hydrogel on wound healing study, the male SD rats (150–180 g) were used in animal study. All animal experiments were performed according to the Guidelines of Institutional Animal Welfare and Research Ethics Committee and conducted following the protocols approved by the Animal Care and Use Committee of Donghua University. After anesthetizing and shaving, a full-thickness wound (diameter of 1 cm) was established. The wounds were treated with gauze, GM/ODex hydrogels, and GM/ODex-APLGA hydrogels. The hydrogel precursor was injected into the wound site by using a medical syringe, followed by UV light exposure for complete gelling. All rats were sacrificed at 14 d post-surgery. The wound tissues were collected and immersed in a 4% paraformaldehyde solution for further histological and immunohistochemical examinations. The hematoxylin and eosin (H&E), Masson's trichrome and CD31 staining were performed.

2.12. Statistical analysis

All data were presented as mean ± standard deviation (SD). A one-way analysis of variance (ANOVA) was used to determine differences. $p < 0.05$ (*) was considered to be significant. $p < 0.01$ (**) was particularly significant.

3. Results and discussion

3.1. Preparation and characterization of segmented APLGA fibers

PLGA was chosen for the preparation of fiber segments due to its good biocompatibility, biodegradability, and mechanical properties. In previous studies, ultrasonication,[42] milling,[43] and cryo-cutting[44] were used to fabricate short fibers. However, the hydrophobic feature of PLGA makes it difficult to disperse evenly in the hydrogel solution. In this work, to get better dispersion, APLGA short fibers were prepared by aminolysis treatment of the PLGA membrane followed by homogenization. During aminolysis treatment, the amino groups ($-NH_2$) at one end of 1,6-hexanediamine react with the ester groups (–COO–) to form a stable amide bond (–CO-NH–), while the amino groups at the other end remained free, which could increase the surface hydrophilicity and provide reactive groups for the subsequent reaction.[45] The hydrophilic APLGA fibers would show better dispersion in an aqueous PVA solution during homogenization. Therefore, aminolysis treatment in combination with homogenization would be able to fabricate fiber segments with shorter length and better uniformity. The microstructures of the PLGA fibrous membrane before (Fig. S1†) and after (Fig. 1a) aminolysis were observed by SEM. Both fibers showed a smooth and uniform morphology, and the average diameters were 2.6 μm and 2.5 μm respectively (Fig. S2†). The chemical structure of APLGA was analyzed by FT-IR and XPS spectroscopy, as shown in Fig. 1b and c, respectively. FT-IR spectra showed that the amino group absorption peak appeared at around 3380 cm^{-1} in the APLGA spectra compared with that of the PLGA spectra. The peak at 1633 cm^{-1} was assigned to the amide carbonyl (C═O) stretching (amide I) and the peak at 1580 cm^{-1} was attributed to the secondary N–H amide bending vibration (amide II). In the XPS spectra, the characteristic signal of N 1s was clearly distinguished at 399.8 eV, confirming the presence of the amino group. These results indicated successful functionalization of PLGA fibers with amino groups, and the modification did not affect the fiber integrity.

The fabrication of satisfactory filler-reinforced hydrogels requires the homogeneous incorporation of fillers. It is well known that micro/nanomaterials still face the challenge of achieving uniform dispersion in the polymer matrix due to easy agglomeration. However, the dispersion state of micro or nano-sized fillers in polymers is a vital factor affecting the mechanical properties of composites.[46] When the PLGA short fibers were physically encapsulated in hydrogels, the hydrophobic PLGA short fibers could not be well mixed with hydrophilic polymers due to the van der Waals forces. To solve this problem, PLGA short fibers were modified by the introduction of amino groups. It was found that the surface of the pristine PLGA membrane was hydrophobic with a WCA of 134.6°, within 30 s (Fig. 1d). In contrast, the WCA of the APLGA membrane decreased significantly to an angle of 19.5° within 30 s, indicating that the PLGA membrane surface became hydrophilic after aminolysis treatment.

Next, the fibrous mats were homogenized to prepare the segmented fibers. From the SEM images, it can be seen that APLGA short fibers displayed shorter lengths and more uniform length distribution compared with PLGA short fibers, which were only mechanically homogenized (Fig. 1e and f). Then, the average length and diameter of the fiber segments

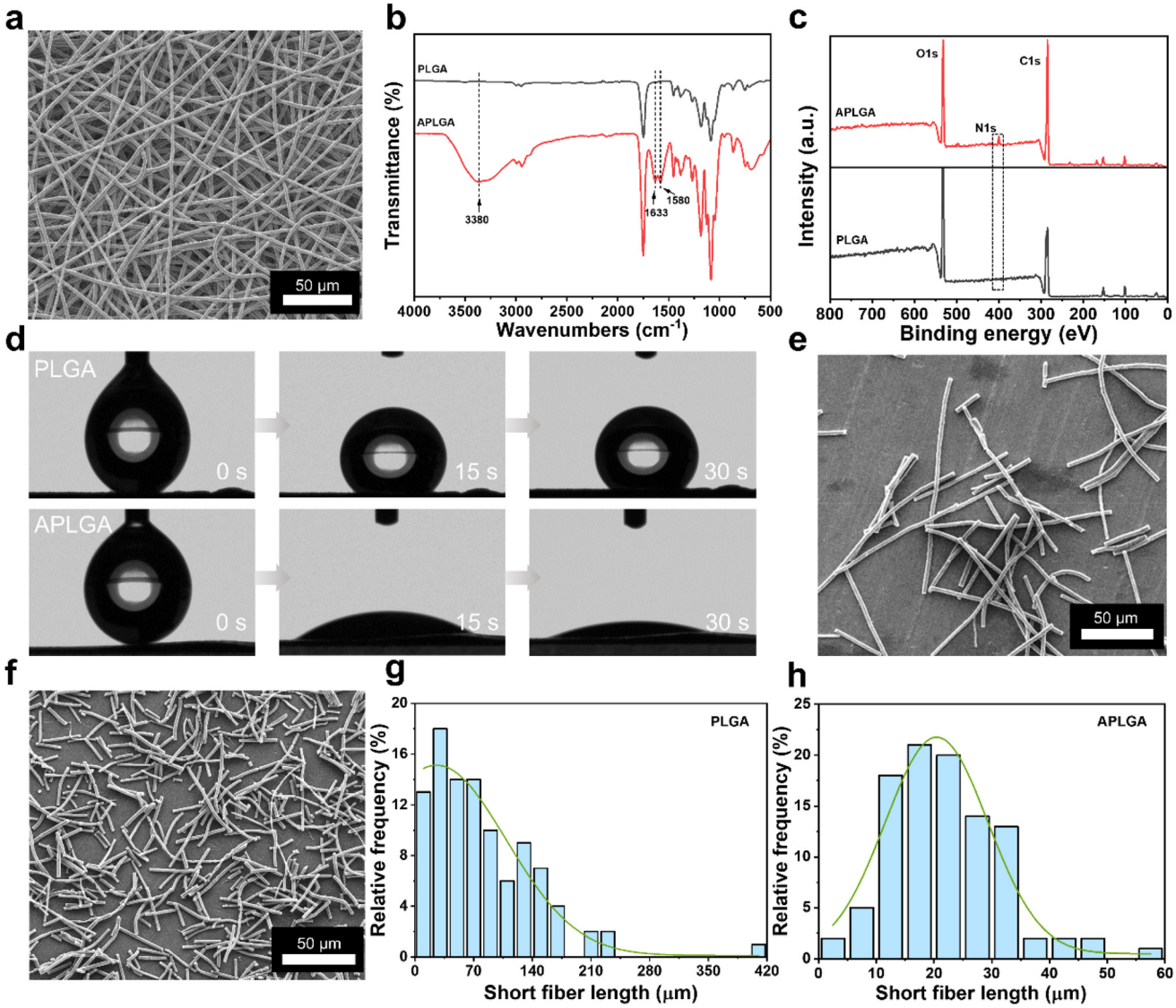

Fig. 1 Fabrication of electrospun fiber segments. (a) SEM image of APLGA electrospun membrane. (b) FT-IR spectra and (c) XPS spectra of PLGA and APLGA membranes. (d) Water contact angle test. SEM images of (e) PLGA and (f) APLGA fiber segments. Length distribution plots of (g) PLGA and (h) APLGA fiber segments.

were measured. The mean length and diameter of PLGA fiber segments were 81.8 μm and 2.6 μm respectively (Fig. 1g and S3a†). In comparison, APLGA fiber segments exhibited a mean length of 22.2 μm with a diameter of 2.4 μm (Fig. 1h and S3b†). Also, the APLGA fiber segments showed higher uniformity. Additionally, we explored the influence of homogenization time on the dispersion of short fibers. Fig. S4† shows the optical microscope images of APLGA fiber segments upon 5 min, 10 min, and 15 min of homogenization. After homogenization of 5 min, a lot of fiber aggregates were observed in the aqueous solution, suggesting that too short homogenization time was insufficient to fully separate the fibers. In contrast, dispersed short fibers were obtained with prolonged homogenization time. The average fiber segment length after 10 min and 15 min of homogenization was about 24.0 μm and 22.6 μm, respectively, suggesting that the fiber segment length was similar to that with a longer homogenization time of 15 min. Therefore, the homogenization time of 10 min was used in the following experiments. Fig. S5† shows the photographs of the short fiber dispersed GM/ODex hydrogel solution. Obvious delamination was seen in the PLGA short fiber solution. In contrast, uniform dispersion was observed in the APLGA short fiber solution. These results indicated that aminolysis treatment followed by optimized homogenization could ensure uniform dispersion of the fiber segments in the hydrogel solution.

3.2. Fabrication and characterization of short fiber–hydrogel composites

The fabrication of short fiber-embedded hydrogels is depicted in Fig. 2a. By introducing short APLGA fibers into the GM/

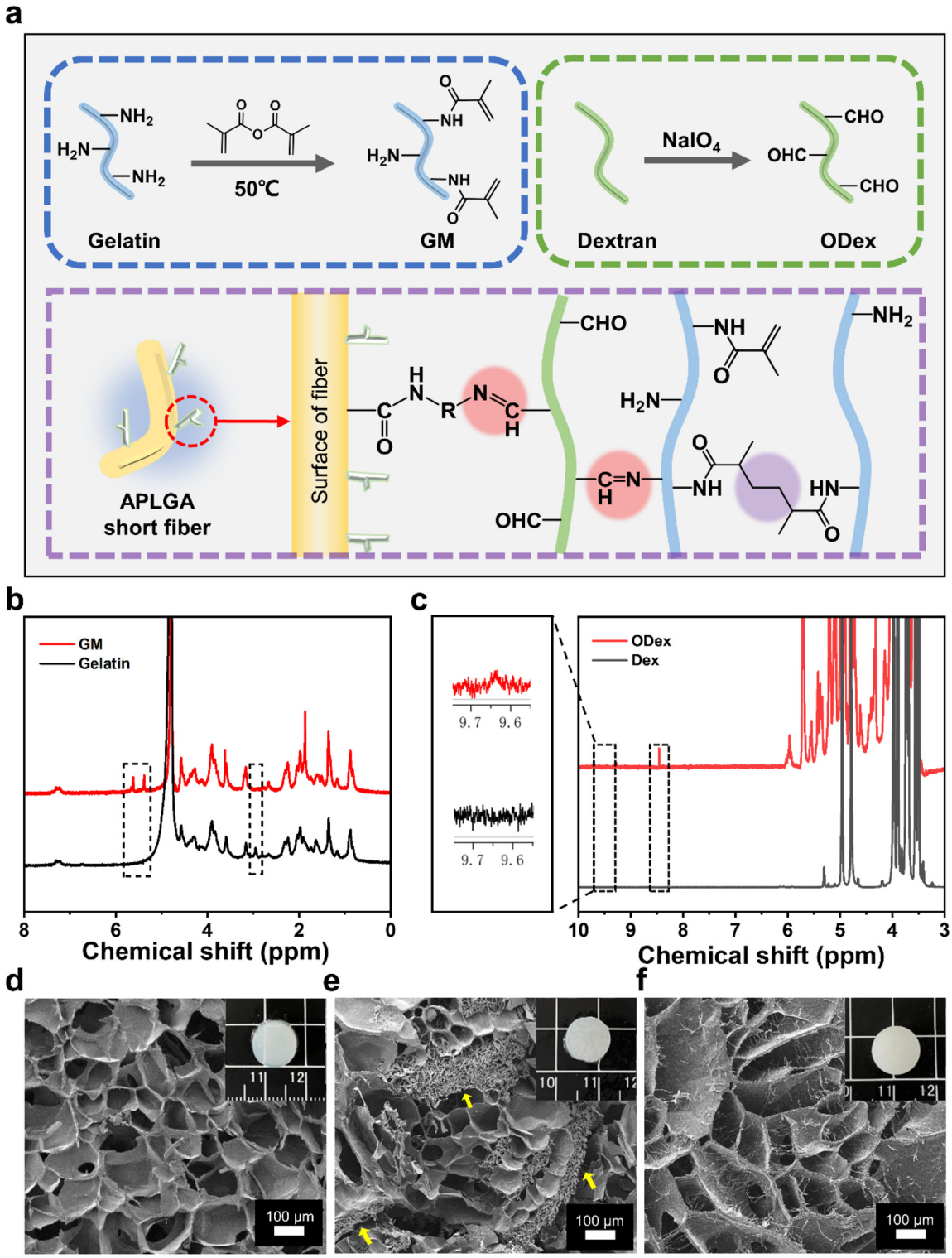

Fig. 2 Synthesis and structural characterization of the short fiber–hydrogel composite. (a) Schematic illustration of the synthesis of GM and ODex and formation of short fiber–hydrogel composite with double crosslinking networks. ^{1}H-NMR spectra of (b) GM, and (c) ODex. SEM images of (d) GM/ODex hydrogel, (e) GM/ODex-PLGA fiber composite, and (f) GM/ODex-APLGA fiber composite. The yellow arrows in (e) indicate aggregated PLGA fibers.

ODex solution, the amino groups of APLGA short fibers as well as GM chains react with the aldehyde groups of ODex to from Schiff-base bonds. To improve the stability, UV-initiated polymerization was carried out for free-radical polymerization of vinyl groups in GM chains. Therefore, the double-crosslinked fiber–hydrogel was formed consisting of dynamic

Schiff-base bonds and nondynamic photo-crosslinking bonds. GM was obtained by modifying gelatin with methacrylic anhydride. Dextran with aldehyde groups was synthesized *via* oxidation by sodium periodate. Fig. 2b shows the ^{1}H-NMR spectra of gelatin and GM. Two new characteristic peaks were observed at 5.61 and 5.38 ppm, corresponding to double-bonded protons of methacrylic anhydride. Meanwhile, the signal of free lysine at 2.95 ppm was significantly decreased, confirming the synthesis of GM.[47] The substitution degree of methacryloyl was about 79.8% as determined from the ^{1}H-NMR spectra. Fig. 2c shows the ^{1}H-NMR spectra of dextran and ODex. The characteristic peaks could be seen at 9.60–9.65 ppm and 8.45–8.50 ppm, which corresponded to the aldehyde group.[48] And the peaks at 4.10–5.70 ppm were attributed to the hemiacetal group, indicating successful oxidation of dextran.[49] The degree of oxidation of ODex was 62.4%, which was measured by the hydroxylamine hydrochloride titration method. The photographs of pristine hydrogel, PLGA fiber–hydrogel, and APLGA fiber–hydrogel showed distinct morphologic features (insets of Fig. 2d–f). The pristine hydrogel was more transparent. However, with the addition of short fibers, the composite hydrogels became opaque. The APLGA fiber–hydrogel showed more homogeneous transparency compared with the PLGA fiber–hydrogel, indicating the uniform distribution of APLGA fiber in the hydrogels. As shown in SEM images, all the freeze-dried hydrogels exhibited porous structures (Fig. 2d–f). With the addition of PLGA fibers, the internal structure of the hydrogel was destroyed due to the aggregation of PLGA fibers. A large number of irregular island-shaped domains composed of short fibers was observed in the hydrogel scaffold, as indicated by the yellow arrows. The fiber aggregation could be caused by the hydrophobic interaction of PLGA fibers. In contrast, the APLGA fiber–hydrogel composites showed a uniform porous structure with the presence of short fibers. Overall, the hydrophilic modification of fibers and the formation of dynamic covalent bonds between the short fibers and hydrogel ensured homogeneous dispersion of short fibers, leading to the formation of uniform short fiber-embedded hydrogels.

3.3. Gelation performances and mechanical properties

Fast gelation is essential in the injectable hydrogel application. Unfortunately, the addition of fillers always delays gelling since the fillers would hinder the hydrogel reaction. Therefore, the fibers were functionalized to form Schiff-base bonds with the hydrogel matrix in this study. Successive photographs were taken to display the gelation process, and the gelation times of hydrogels with or without fibers were recorded *via* the vial inversion method (Fig. 3a). The pristine GM/ODex solution and PLGA fiber incorporated GM/ODex solution were still in the liquid state after 20 min. In contrast, the solution containing APLGA short fibers showed a gelling tendency in 15 min and a solid gel was formed after 20 min. These findings indicated that the interfacial reaction between APLGA fibers and ODex could contribute to faster gelling. Notably, in combination with UV-assisted crosslinking, the gelation time was shortened to 90 s (Fig. 3b). The light-curing ability allowed

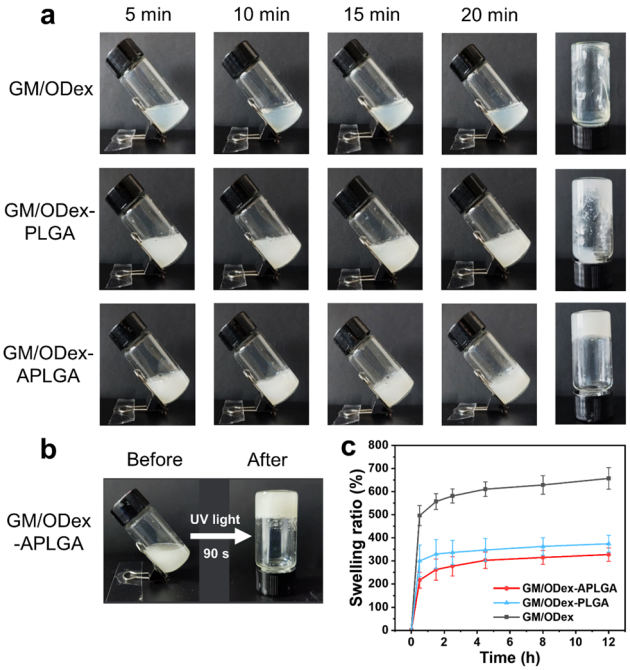

Fig. 3 Gelation and swelling ability of the short fiber–hydrogel composite. (a) Photographs showing the gelling process of the GM/ODex, GM/ODex-PLGA, and GM/ODex-APLGA hydrogels. (b) Photographs showing gelling of the GM/ODex-APLGA hydrogels under UV irradiation. (c) The swelling ratio of different hydrogels.

rapid gelling and spatiotemporal control of hydrogel formation. The fast gelation feature of the double-crosslinked fiber–hydrogels would ensure their *in situ* application.

The swelling behavior of hydrogels is of importance for wound dressing materials since the hydrogels can absorb excess tissue exudate while maintaining a favorable moist environment. However, too much liquid can diminish the stability or even destroy the hydrogel network. Therefore, an appropriate swelling property is critical for hydrogel dressings.[50] Fig. 3c shows the swelling-ratio curves of hydrogels with increasing incubation times. The GM/ODex hydrogels displayed the highest swelling rate of 657.1% after 12 h. However, the GM/ODex-APLGA fiber composites presented the lowest swelling rate of 327.2%, which could be ascribed to the dense crosslinking network.

Injectable and *in situ* forming behavior of hydrogels is essential for the treatment of irregular wounds. As shown in Fig. 4a, the short fiber–hydrogel solution could easily pass through a 22 G needle without clogging. The short fiber–hydrogel composite could be shaped into robust shapes, such as a heart and a star. In addition, the injectable feature and rapid gelation capability under UV irradiation allowed the smooth writing of letters. These results demonstrated the great potential of injectable hydrogel for covering irregular wounds.

We explored the rheological performance of different hydrogels. Fig. 4b shows the strain sweep measurement of GM/ODex-APLGA hydrogels with strains ranging from 0.1 to 100%. The crossover points of G' and G'' indicated the critical strain

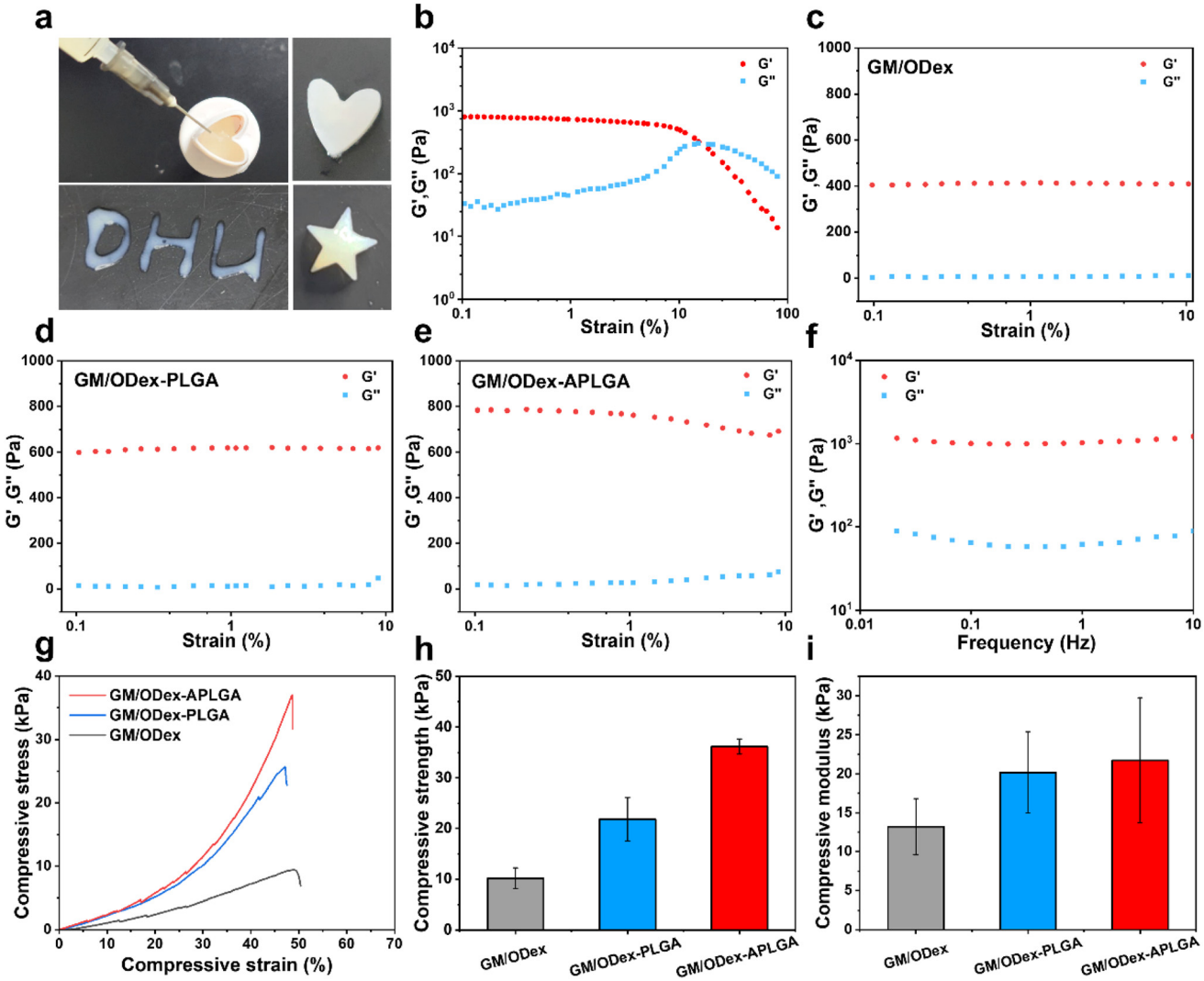

Fig. 4 Injectability and mechanical property of short fiber–hydrogel composites. (a) Photographs showing the injectable and *in situ* forming properties of GM/ODex-APLGA hydrogels. (b) Strain sweep test of GM/ODex-APLGA hydrogels. *G′* and *G″* of (c) GM/ODex, (d) GM/ODex-PLGA, and (e) GM/ODex-APLGA hydrogels. (f) Oscillatory frequency sweep test of GM/ODex-APLGA hydrogels. (g) Compressive stress–strain curves of GM/ODex, GM/ODex-PLGA, and GM/ODex-APLGA hydrogels, and corresponding (h) average compressive strength and (i) average compressive modulus.

of about 15.1%, which suggested the transformation of the hydrogel to a quasi-liquid. With increasing strain, the *G′* value decreased remarkably, which was lower than the *G″* value, indicating the collapse of the hydrogel network. The *G′* of GM/ODex-APLGA hydrogels was about 2.0 and 1.3 times that of GM/ODex and GM/ODex-PLGA hydrogels, respectively (Fig. 4c–e). In addition, the oscillatory frequency sweep measurement of GM/ODex-APLGA hydrogels at the frequency of 0.01–10 Hz is shown in Fig. 4f. *G′* remained higher than *G″*, suggesting a stable hydrogel network. These findings suggested that the crosslinking density and stiffness of fiber–hydrogel composites were enhanced by incorporating APLGA short fibers with interfacial bonding to the hydrogel.

The hydrogel dressing applied on the wound site should withstand a certain external compression of the surrounding tissues during movement. Therefore, wound dressings require suitable compressive capability to maintain their structural integrity. The compressive property of double-crosslinked hydrogels was investigated by compression tests. As shown in Fig. 4g, the introduction of PLGA fiber segments into the hydrogels showed an increase in compressive strength (21.8 kPa) as compared with pristine GM/ODex hydrogel (10.2 kPa), due to the reinforcement of fiber fillers. In contrast, the GM/ODex-APLGA hydrogels exhibited the highest compressive strength of 36.2 kPa (Fig. 4h) and compressive modulus of 21.7 kPa (Fig. 4i). Fig. S6† shows the photographs of GM/ODex-APLGA hydrogels before and after compression. These results indicated that the addition of electrospun fiber fillers and formation of double-crosslinked network contributed to improved mechanical properties.

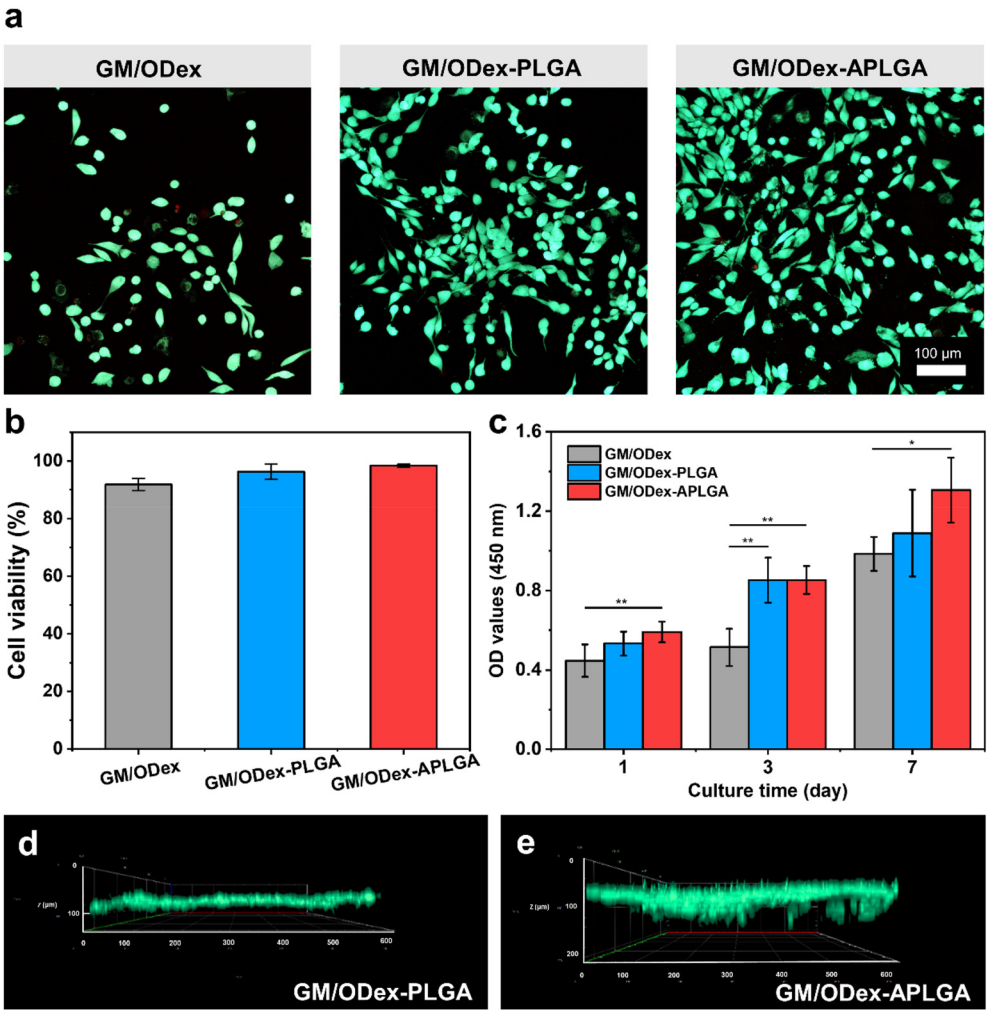

Fig. 5 The cytocompatibility of hydrogels. (a) Live/dead staining of L929 cells after 3 d of culture on GM/ODex, GM/ODex-PLGA, and GM/ODex-APLGA hydrogels. (b) Cell viability. (c) Cell proliferation by CCK-8 assay. Data are presented as mean ± SD (n = 4), *p < 0.05, **p < 0.01. 3D confocal images of L929 fibroblasts cultured on (d) GM/ODex-PLGA, and (e) GM/ODex-APLGA hydrogels.

3.4. *In vitro* assessment of cytocompatibility

To assess the biocompatibility of the composite hydrogel, L929 fibroblasts were cultured on the hydrogels. Fig. 5a shows the live/dead staining after incubating for 3 d. More cells were observed in the GM/ODex-PLGA and GM/ODex-APLGA hydrogels as compared with GM/ODex hydrogels, indicating that the presence of fibers in the hydrogels facilitated cell adhesion and growth. The quantitative analysis showed that all hydrogels supported a high cell viability greater than 90% (Fig. 5b), suggesting excellent biocompatibility. Cell proliferation property was evaluated *via* the CCK-8 assay. As shown in Fig. 5c, the GM/ODex-APLGA hydrogels showed the highest cell proliferation. It is well known that it is difficult for hydrogels to simulate the nanofibrous structures of the ECM, resulting in the restriction of cell infiltration, migration, and proliferation.[51] However, the addition of fiber segments is able to introduce a fibrous structure, rearrange the internal microstructure of the hydrogel and roughen the hydrogel surface, which may provide more adherent sites for cells and support cell proliferation.[52] Fig. 5d and e show the 3D confocal images of GM/ODex-PLGA and GM/ODex-APLGA hydrogels after 3 d of culturing. It can be seen that the cells could infiltrate the hydrogels, demonstrating that the hydrogels with fibers facilitated cell growth inside. In addition, a higher infiltration depth was observed in the GM/ODex-APLGA hydrogel. Previous research found that the electrospun fiber embedded hydrogels could enhance cell migration and infiltration due to the high porosity and addition of nanofibers.[53] The results in this study indicated that the uniform distribution of pore structure and short fibers were helpful for cell infiltration.

3.5. *In vivo* wound healing efficacy

To explore the wound healing capability of GM/ODex-APLGA hydrogel, an *in vivo* study was performed *via* a rat full-thickness skin defect model. The GM/ODex and GM/ODex-APLGA hydrogels were *in situ* formed in the wound sites, with gauze dressing as the control. All wounds showed a trend of gradual healing without infection. As shown in Fig. 6a and b, the GM/ODex-APLGA group

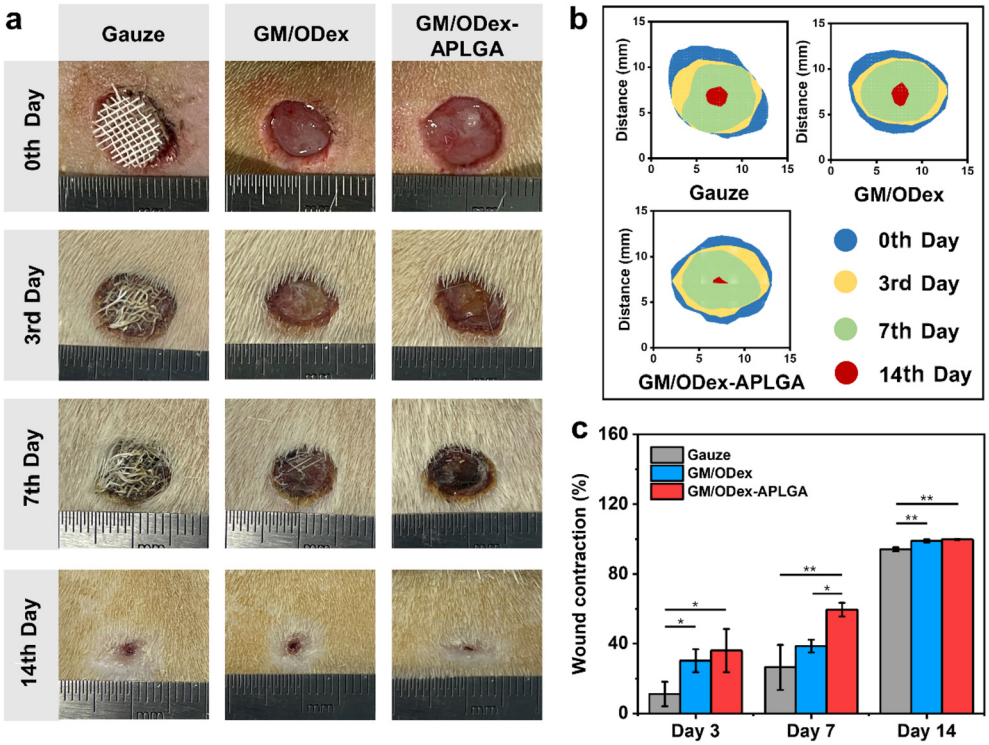

Fig. 6 Wound healing performance of hydrogel–fiber composites. (a) Photographs of wounds treated with gauze, GM/ODex hydrogel, and GM/ODex-APLGA hydrogel at 0th, 3rd, 7th, and 14th day post-surgery. (b) Traces of remaining wound area during 14 days. (c) Contraction ratio of wounds. Data are presented as mean ± SD (n = 3), *p < 0.05, **p < 0.01.

displayed a smaller wound area than gauze and GM/ODex groups. At 14 d, the wound contraction rate of the GM/ODex-APLGA hydrogel group reached 99.8%, which was higher than that of the gauze group (94.2%) and GM/ODex group (99.0%).

The wound tissues collected at the 14th day post-surgery were analyzed by H&E (Fig. 7a), Masson's trichrome (Fig. 7b), and CD31 (Fig. 7c) staining. The H&E staining showed that the comparatively intact epithelial tissue and more mature granu-

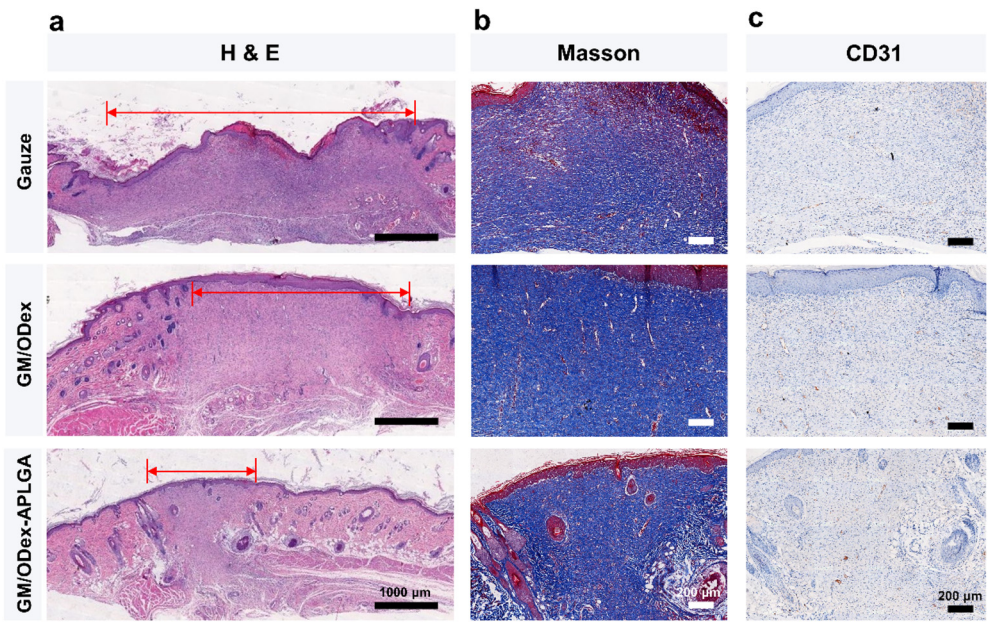

Fig. 7 Histological evaluation of regenerated tissue at the wounds after treated with gauze, GM/ODex hydrogel, and GM/ODex-APLGA hydrogel. (a) H&E stained, (b) Masson stained, and (c) CD31 stained images of wound tissue on the 14th day post-surgery.

lation were observed in the GM/ODex-APLGA hydrogel group after 14 d. For Masson's trichrome staining, sparse collagen deposition was observed in the control group, whereas the GM/ODex-APLGA hydrogel group possessed more organized collagen fibers which were similar to normal skin tissues. Angiogenesis in regenerated wound tissues was evaluated by immunohistochemical staining with CD31. It was observed that stronger CD31 expression appeared in the tissue sections of the GM/ODex-APLGA group, indicating better vascularization. Overall, the GM/ODex-APLGA hydrogel treated wounds showed rapid re-epithelialization, organized collagen deposition, and high angiogenesis, indicating that the APLGA fiber segment-embedded hydrogels effectively promoted wound healing.

Wound healing requires a series of events involving cells, growth factors, and extracellular matrix.[54] Therefore, the ideal wound dressing would provide suitable microenvironment for wound healing. The GM/ODex-APLGA hydrogels possessed a good injectable ability and *in situ* forming feature, providing perfect coverage of the skin defects. In addition, the short fiber–hydrogel composite could keep a moist healing environment. The fiber segment reinforced hydrogels with a uniform and stable network structure and adjustable mechanical performance could withstand deformation. Besides, the introduction of the APLGA short fibers with improved affinity offered ECM mimetic architecture, which facilitate cell proliferation and infiltration, accelerating reconstruction of damaged tissues. Therefore, the *in vivo* study demonstrated that the GM/ODex-APLGA fiber–hydrogel could be a promising candidate as wound dressing material.

4. Conclusions

An injectable *in situ* forming fiber-incorporated hydrogel was developed in this study. The amino-modified electrospun PLGA short fibers with improved hydrophilicity and uniform distribution showed good dispersion in aqueous solution. The double-crosslinked hydrogels were formed through a Schiff-base reaction between short fibers and the hydrogel matrix followed by photo-induced radical polymerization of the hydrogel matrix. The presence of APLGA fibers in the hydrogels provided better biomimicking of the ECM structure. Compared with PLGA short fibers, the introduction of APLGA short fibers with a uniform length and high dispersibility resulted in better compressibility of the composite hydrogels. Furthermore, the structural biomimetic GM/ODex-APLGA hydrogels effectively promoted cell proliferation and infiltration. Moreover, the *in vivo* study showed that GM/ODex-APLGA hydrogels improved wound healing. These results indicated that the injectable *in situ* forming GM/ODex-APLGA hydrogels could be a great potential candidate in the field of irregular wound treatment.

Conflicts of interest

There are no conflicts to declare.

Acknowledgements

This work was supported by the Ministry of Science and Technology of China (2021YFE0105100), the National Natural Science Foundation of China (52073055, 51925302, and 51973028), the National Center for Research and Development (NCBiR) (WPC2/NanoHealer/2021), the Fundamental Research Funds for the Central Universities and DHU Distinguished Young Professor Program (LZA2021001).

References

1 Y. Wang, R. Xie, Q. Li, F. Dai, G. Lan, S. Shang and F. Lu, *Biomater. Sci.*, 2020, **8**, 1910–1922.
2 T. Wang, Y. Li, E. J. Cornel, C. Li and J. Du, *ACS Nano*, 2021, **15**, 9027–9038.
3 Y. Yang, L. Chen, M. Sun, C. Wang, Z. Fan and J. Du, *Chin. J. Polym. Sci.*, 2021, **39**, 1412–1420.
4 S. Correa, A. K. Grosskopf, H. L. Hernandez, D. Chan, A. C. Yu, L. M. Stapleton and E. A. Appel, *Chem. Rev.*, 2021, **121**, 11385–11457.
5 Y. Liang, J. He and B. Guo, *ACS Nano*, 2021, **15**, 12687–12722.
6 J. Xiao, Y. Zhou, M. Ye, Y. An, K. Wang, Q. Wu, L. Song, J. Zhang, H. He, Q. Zhang and J. Wu, *Adv. Healthcare Mater.*, 2021, **10**, e2001591.
7 S. Du, B. Liu, Z. Li, H. Tan, W. Qi, T. Liu, S. Qiang, T. Zhang, F. Song, X. Chen, J. Chen, H. Qiu and W. Wu, *ACS Appl. Bio. Mater.*, 2021, **4**, 4522–4531.
8 X. Zhao, L. Liu, T. An, M. Xian, J. A. Luckanagul, Z. Su, Y. Lin and Q. Wang, *Acta Biomater.*, 2020, **104**, 85–94.
9 V. A. T. Le, T. X. Trinh, P. N. Chien, N. N. Giang, X. R. Zhang, S. Y. Nam and C. Y. Heo, *Polymers*, 2022, **14**, 919.
10 D. Liu, Y. Liao, E. J. Cornel, M. Lv, T. Wu, X. Zhang, L. Fan, M. Sun, Y. Zhu, Z. Fan and J. Du, *Chem. Mater.*, 2021, **33**, 7972–7985.
11 J. Zhang, Y. Zheng, J. Lee, J. Hua, S. Li, A. Panchamukhi, J. Yue, X. Gou, Z. Xia, L. Zhu and X. Wu, *Nat. Commun.*, 2021, **12**, 1670.
12 C. Ghobril and M. W. Grinstaff, *Chem. Soc. Rev.*, 2015, **44**, 1820–1835.
13 J. Qu, X. Zhao, Y. Liang, T. Zhang, P. X. Ma and B. Guo, *Biomaterials*, 2018, **183**, 185–199.
14 B. C. Ilochonwu, M. Mihajlovic, R. F. Maas-Bakker, C. Rousou, M. Tang, M. Chen, W. E. Hennink and T. Vermonden, *Biomacromolecules*, 2022, **23**, 2914–2929.
15 J. H. Wang, C. W. Tsai, N. Y. Tsai, C. Y. Chiang, R. S. Lin, R. F. Pereira and Y. E. Li, *Int. J. Biol. Macromol.*, 2021, **185**, 441–450.
16 M. Cordero, C. Ruiz, D. A. Palacio, P. Turunen, A. Rowan and B. F. Urbano, *Int. J. Biol. Macromol.*, 2022, **204**, 635–643.
17 J. Guo, H. Yao, X. Li, L. Chang, Z. Wang, W. Zhu, Y. Su, L. Qin and J. Xu, *Bioact. Mater.*, 2023, **21**, 175–193.

18 H. Sun, J. Tang, Y. Mou, J. Zhou, L. Qu, K. Duval, Z. Huang, N. Lin, R. Dai, C. Liang, Z. Chen, L. Tang and F. Tian, *Acta Biomater.*, 2017, **48**, 88–99.
19 X. Fang, H. Guo, W. Zhang, H. Fang, Q. Li, S. Bai and P. Zhang, *J. Mater. Chem. B*, 2020, **8**, 10593–10601.
20 J. Park, J. Jeon, B. Kim, M. S. Lee, S. Park, J. Lim, J. Yi, H. Lee, H. S. Yang and J. Y. Lee, *Adv. Funct. Mater.*, 2020, **30**, 2003759.
21 S. Pacelli, R. Maloney, A. R. Chakravarti, J. Whitlow, S. Basu, S. Modaresi, S. Gehrke and A. Paul, *Sci. Rep.*, 2017, **7**, 6577.
22 K. Zhu, S. R. Shin, T. van Kempen, Y. C. Li, V. Ponraj, A. Nasajpour, S. Mandla, N. Hu, X. Liu, J. Leijten, Y. D. Lin, M. A. Hussain, Y. S. Zhang, A. Tamayol and A. Khademhosseini, *Adv. Funct. Mater.*, 2017, **27**, 1605352.
23 A. Navaei, H. Saini, W. Christenson, R. T. Sullivan, R. Ros and M. Nikkhah, *Acta Biomater.*, 2016, **41**, 133–146.
24 A. Paul, V. Manoharan, D. Krafft, A. Assmann, J. A. Uquillas, S. R. Shin, A. Hasan, M. A. Hussain, A. Memic, A. K. Gaharwar and A. Khademhosseini, *J. Mater. Chem. B*, 2016, **4**, 3544–3554.
25 J. Liu, L. Li, H. Suo, M. Yan, J. Yin and J. Fu, *Mater. Des.*, 2019, **171**, 107708.
26 K. Modaresifar, A. Hadjizadeh and H. Niknejad, *Artif. Cells, Nanomed., Biotechnol.*, 2018, **46**, 1799–1808.
27 W. Xu, B. Z. Molino, F. Cheng, P. J. Molino, Z. Yue, D. Su, X. Wang, S. Willfor, C. Xu and G. G. Wallace, *ACS Appl. Mater. Interfaces*, 2019, **11**, 8838–8848.
28 Y. Zhu, Q. Jiang, Z. Jin, D. Chen, Q. Xu, J. Chen, Y. Zeng, S. Chen and Q. He, *Adv. Healthcare Mater.*, 2022, e2201705.
29 J. Huang and Y. Gu, *Curr. Opin. Colloid Interface Sci.*, 2011, **16**, 470–481.
30 F. Ansari and L. A. Berglund, *Biomacromolecules*, 2018, **19**, 2341–2350.
31 Y. Dong, Y. Zheng, K. Zhang, Y. Yao, L. Wang, X. Li, J. Yu and B. Ding, *Adv. Fiber Mater.*, 2020, **2**, 212–227.
32 X. Lu, X. Li, J. Yu and B. Ding, *Acta Biomater.*, 2022, **154**, 49–62.
33 J. Xue, T. Wu, J. Qiu, S. Rutledge, M. L. Tanes and Y. Xia, *Adv. Funct. Mater.*, 2020, **30**, 2002031.
34 J. Xue, T. Wu, Y. Dai and Y. Xia, *Chem. Rev.*, 2019, **119**, 5298–5415.
35 J. Jang, J. Lee, Y.-J. Seol, Y. H. Jeong and D.-W. Cho, *Composites, Part B*, 2013, **45**, 1216–1221.
36 T. D. Stocco, M. C. M. Silva, M. A. F. Corat, G. G. Lima and A. O. Lobo, *Int. J. Nanomed.*, 2022, **17**, 1111–1124.
37 X. Li, C. Zhang, A. E. Haggerty, J. Yan, M. Lan, M. Seu, M. Yang, M. M. Marlow, I. Maldonado-Lasuncion, B. Cho, Z. Zhou, L. Chen, R. Martin, Y. Nitobe, K. Yamane, H. You, S. Reddy, D. P. Quan, M. Oudega and H. Q. Mao, *Biomaterials*, 2020, **245**, 119978.
38 Y. Liu, Q. Wang, X. Liu, P. Nakielski, F. Pierini, X. Li, J. Yu and B. Ding, *ACS Appl. Bio. Mater.*, 2022, **5**, 1047–1056.
39 A. Ovsianikov, A. Deiwick, S. Van Vlierberghe, P. Dubruel, L. Moller, G. Drager and B. Chichkov, *Biomacromolecules*, 2011, **12**, 851–858.
40 G. M. Taboada, P. Dosta, E. R. Edelman and N. Artzi, *Adv. Mater.*, 2022, **34**, 2203087.
41 H. Zhao and N. D. Heindel, *Pharm. Res.*, 1991, **8**, 400–402.
42 H. Y. Wang, Y. Y. Chen and Y. Q. Zhang, *Mater. Sci. Eng., C*, 2015, **48**, 444–452.
43 S. Feng, Z. Zhan, Y. Yi, Z. Zhou and C. Lu, *Composites, Part A*, 2022, **157**, 106907.
44 S. K. Boda, S. Chen, K. Chu, H. J. Kim and J. Xie, *ACS Appl. Mater. Interfaces*, 2018, **10**, 25069–25079.
45 W. Mattanavee, O. Suwantong, S. Puthong, T. Bunaprasert, V. P. Hoven and P. Supaphol, *ACS Appl. Mater. Interfaces*, 2009, **1**, 1076–1085.
46 A. Zengin, J. P. O. Castro, P. Habibovic and S. H. van Rijt, *Nanoscale*, 2021, **13**, 1144–1154.
47 S. Gholizadeh, X. Chen, A. Yung, A. Naderi, M. Ghovvati, Y. Liu, A. Farzad, A. Mostafavi, R. Dana and N. Annabi, *Biomater. Sci.*, 2023, DOI: **10.1039/d2bm01013e**.
48 H. Chen, Z. Ding, D. Yan, H. He, W. Xi, J. Hu, R. Zhang, Y. Yan and Q. Zhang, *Carbohydr. Polym.*, 2022, **296**, 119900.
49 X. Zhao, Y. Yang, J. Yu, R. Ding, D. Pei, Y. Zhang, G. He, Y. Cheng and A. Li, *Biomaterials*, 2022, **282**, 121387.
50 T. Hu, G.-P. Wu, H. Bu, H. Zhang, W.-X. Li, K. Song and G.-B. Jiang, *Chem. Eng. J.*, 2022, **450**, 138201.
51 E. Prince and E. Kumacheva, *Nat. Rev. Mater.*, 2019, **4**, 99–115.
52 A. A. Abalymov, C. A. B. Santos, L. Van der Meeren, D. Van de Walle, K. Dewettinck, B. V. Parakhonskiy and A. G. Skirtach, *Adv. Mater. Interfaces*, 2021, **8**, 2002202.
53 X. Li, B. Cho, R. Martin, M. Seu, C. Zhang, Z. Zhou, J. S. Choi, X. Jiang, L. Chen, G. Walia, J. Yan, M. Callanan, H. Liu, K. Colbert, J. Morrissette-McAlmon, W. Grayson, S. Reddy, J. M. Sacks and H.-Q. Mao, *Sci. Transl. Med.*, 2019, **11**, eaau6210.
54 Q. Zeng, X. Qi, G. Shi, M. Zhang and H. Haick, *ACS Nano*, 2022, **16**, 1708–1733.

